REPORT DOCUMENTATION PAGE

Form Approved OMB NO. 0704-0188

1. REPORT DATE (DD-MM-YYYY)	2. REPORT TYPE	3. DATES COVERED (From - To)
11-09-2019	Final Report	16-Jun-2018 - 11-Jun-2019

4. TITLE AND SUBTITLE
Final Report: OAM and Quantum Penetrating Radar

5a. CONTRACT NUMBER
W911NF-18-1-0193

5b. GRANT NUMBER

5c. PROGRAM ELEMENT NUMBER
611103

6. AUTHORS

5d. PROJECT NUMBER

5e. TASK NUMBER

5f. WORK UNIT NUMBER

7. PERFORMING ORGANIZATION NAMES AND ADDRESSES
University of Vermont
85 South Prospect Street, 340 Waterman Building

Burlington, VT 05405 -0160

8. PERFORMING ORGANIZATION REPORT NUMBER

9. SPONSORING/MONITORING AGENCY NAME(S) AND ADDRESS (ES)
U.S. Army Research Office
P.O. Box 12211
Research Triangle Park, NC 27709-2211

10. SPONSOR/MONITOR'S ACRONYM(S)
ARO

11. SPONSOR/MONITOR'S REPORT NUMBER(S)
72227-EL-RIP.3

12. DISTRIBUTION AVAILIBILITY STATEMENT
Approved for public release; distribution is unlimited.

13. SUPPLEMENTARY NOTES
The views, opinions and/or findings contained in this report are those of the author(s) and should not contrued as an official Department of the Army position, policy or decision, unless so designated by other documentation.

14. ABSTRACT

15. SUBJECT TERMS

16. SECURITY CLASSIFICATION OF:			17. LIMITATION OF ABSTRACT	15. NUMBER OF PAGES	19a. NAME OF RESPONSIBLE PERSON
a. REPORT	b. ABSTRACT	c. THIS PAGE			Dryver Huston
UU	UU	UU	UU		19b. TELEPHONE NUMBER 802-656-1922

RPPR Final Report
as of 14-Nov-2019

Agency Code:

Proposal Number: 72227ELRIP **Agreement Number: W911NF-18-1-0193**
INVESTIGATOR(S):

Name: Dryver Huston
Email: dryver.huston@uvm.edu
Phone Number: 8026561922
Principal: Y

Name: Tian Xia
Email: txia@uvm.edu
Phone Number: 8026568996
Principal: N

Organization: **University of Vermont**
Address: 85 South Prospect Street, 340 Waterman Building, Burlington, VT 054050160
Country: USA
DUNS Number: 066811191 EIN: 030179440

Report Date: 11-Sep-2019 Date Received: 11-Sep-2019
Final Report for Period Beginning 16-Jun-2018 and Ending 11-Jun-2019
Title: OAM and Quantum Penetrating Radar
Begin Performance Period: 16-Jun-2018 **End Performance Period:** 11-Jun-2019
Report Term: 0-Other

Submitted By: Dryver Huston Email: dryver.huston@uvm.edu
Phone: (802) 656-1922

STEM Degrees: 0 **STEM Participants:** 2

Major Goals: The goal of this project was to acquire microwave test equipment and to assemble a test bed to enable research into high-performance ground and wall penetrating radars and related topics. The emphasis is on the use of digital control, orbital angular momentum (OAM) control and the exploitation of quantum effects.

The following is a brief description of the equipment originally proposed for acquisition.

The first piece of equipment was a PXIe-based time-domain-synchronized 2-input 2-output microwave transmit/receive system, along with a 3 GHz RF Vector Signal generator. This system has four main components: 1. A PXIe 18-slot 24GB/s instrument rack that houses instrument modules for the rest of the system. The rack and modules contain an onboard PC controller and provide a custom instrument control programming environment. The availability of extra memory slots allows for expansion to add more modules. 2. A Two-Channel 1 GSPS 14-bit PXI Arbitrary Waveform Generator. 3. A Two Channel, 14-bit, 500 MHz GS/s PXIe Digitizer. And 4. MXG X-Series RF Vector Signal Generator. Some details are:

1. PXIe 10-slot 8GB/s Instrument Rack:
a. PXIe Chassis: PXIe Chassis 10-slot, 3U, 24GB/s (Keysight M9019A $4,226); b. PXIe Embedded Controller: with Intel i7, 4 GB RAM, 240 GB SSD, Windows Embedded Standard 7 (64 bit), Memory, 16GB (Keysight M9037A $6,898), c. HVI Programming Environment (Keysight M3601A $1,692), and d. Graphical FPGA Design Environment (Keysight M3602A $2,542); Total ($15,358).
b. PXI Arbitrary Waveform Generator: Two channel 1 GSPS, 14 bits with Dual modulation capability (amplitude and angle), Enabled FPGA programming, Enabled HVI programming, Variable sampling clock, Xilinx FPGA, 2 GB Memory, (Keysight M3202A $16,483).
c. PXIe Digitizer: Two Channel, 14-bit, DC Coupled, 500 MHz bandwidth, Memory, 2GB, with HVI and FPGA programmability (Keysight M9203A $0 special discount).
2. MXG X-Series RF Vector Signal Generator: Two channel, LO in/out for phase coherency, High output power, Multifunction generator, Frequency range, 9 kHz to 3 GHz, ARB baseband generator (80 MHz RF bandwidth, baseband generator with real-time capability, AM, FM, phase modulation, Narrow pulse modulation, Enhanced low phase noise (Keysight N5182B $64,376)

3. Total Price: $96,216

In addition to the above equipment, it was proposed to acquire accessories to support these instruments, including custom-machined waveplates and antennas for generating and receiving microwaves photons with controlled OAM, and leading to experiments based on electromagnetic wave shape control, hyperentanglement and frequency-domain entanglement. The funding for supplies in the amount of $1,333 was for the purchase of microwave cables, probes, mixers, absorbing foam and switches to support using the test equipment.

Five anticipated uses of the equipment are: 1. A system to support research into the digital control of time and frequency content of classical penetrating radar systems. This includes multi-static and phased array configurations, time and frequency domain compressive radar sensing, and software defined cognitive penetrating radar systems. 2. A system to support research into the use of controlled OAM microwaves, along with related quantum effects to improve the performance of penetrating radars. 3. A testbed for applied problems that can benefit from controlled OAM microwave radars including the location and classification of buried objects, determining the structural characteristics of walls, locating objects behind walls, operating orthogonal antenna arrays, and the operation of penetrating radars in electromagnetically challenging environments. 4. A testbed for related microwave research, such as software-defined radio communications. 5. Serve as an educational tool for students working in areas of microwave engineering, sensing, cognitive systems and structural identification.

Accomplishments: The following is a brief description of the equipment purchased as part of this project. The acquired equipment was similar to the proposed configuration but differed in performance specifications, number of items and testbed configuration. This included a 4-channel arbitrary waveform generator source instead of the original 2-channel version, and an increase in the frequency range of the RF Vector Signal Generators from 3 GHz to 6 GHz to provide better support for making microwaves with OAM using phased array methods, instead of the originally proposed wave plates. Better pricing from the vendor was the primary reason for the difference. Details follow:

1. PXIe 10-slot 8GB/s Instrument Rack and Modules:
a. PXIe Chassis PXIe Chassis 10-slot, 3U, 24GB/s (Keysight M9019A $4,418.11); b. PXIe Embedded Controller: with Intel i7, 4 GB RAM, 240 GB SSD, Windows Embedded Standard 7 (64 bit), Memory, 16GB (Keysight M9037A $7,207.67), c. HVI Programming Environment (Keysight M3601A $1,768.00), and d. Graphical FPGA Design Environment (Keysight M3602A $2,656.25); Total ($16,050.03).
b. PXI Arbitrary Waveform Generator: Four channel 1 GSPS, 14 bits with Dual modulation capability (amplitude and angle), Enabled FPGA programming, Enabled HVI programming, Variable sampling clock, FPGA, Xilinx, Memory, 2 GB, (Keysight M3202A $17,300.90).
c. PXIe Digitizer: Four Channel, 14-bit, DC Coupled, 500 MHz bandwidth, 2 GB Memory, with HVI and FPGA programmability (Keysight M3102A $0 special discount).
2. MXG X-Series RF Vector Signal Generators: Two units, LO in/out for phase coherency, High output power, Multifunction generator, Frequency range, 9 kHz to 6 GHz, ARB baseband generator (80 MHz RF bandwidth, baseband generator with real-time capability, AM, FM, phase modulation, Narrow pulse modulation, Enhanced low phase noise (Keysight N5182B $62,467.50)
3. Total Price: $95,818.43

In addition to the equipment a set of supplies in the form of cables, splitters, phase shifters, mixers, antennas and lumber for the purpose of setting up a testbed for the generation and reception of OAM waves. This is a 4-channel send to 4-channel receive system.

The testbed has the following features:
1. Location on the same PXIe bus synchronizes the 4-channel source and 4-channel receiver/digitizer to run on the same clock. This minimizes noise due to jitter and timing drift.
2. The antennas are log period PCB boards from Kent Electronics (Model LP0410) with a 400 MHz to 1 GHz bandwidth at 5-6dBi Gain. The far-field electric polarization is parallel to the plane of the board.
3. The pegboard construction allows for rapid reconfiguration of geometry and polarization.

The equipment works as expected. Experiments with the equipment indicate that it may be possible to produce microwave beams with OAM using phased-array techniques and that these beams may exhibit behaviors behind obstructions that differs from beams without OAM.

Training Opportunities: This equipment will serve as an educational tool for students working in areas of microwave engineering, sensing, cognitive systems and structural identification.

To date this equipment has been used primarily by University of Vermont Mechanical Engineering graduate student Daniel Orfeo. Experiments conducted with this equipment will form a principal component of this Ph.D. dissertation.

In addition, one post-doctoral fellow and two undergraduate engineering students have had some experience with this equipment.

Results Dissemination: Research using equipment acquired as part of this project has appeared in the following conference publications:

Orfeo D, Ezequelle W, Xia T, Huston DR. (2019) “Orbital Angular Momentum Assisted Ground Penetrating Radar” SPIE Defense + Commercial Sensing Symposium Detection and Sensing of Mines, Explosive Objects, and Obscured Targets XXIV, paper no. 11012-47, Baltimore, MD, DOI:10.1117/12.2520545

Orfeo D, Burns D, Xia T, Huston D. (2019) “Phased Array for Control of Orbital Angular Momentum in Microwave Systems” IEEE 2019 IEEE International Symposium on Phased Array Systems and Technology, Waltham, MA, USA

Honors and Awards: Nothing to Report

Protocol Activity Status:

Technology Transfer: Some of the experiments using this equipment received support from other sources. A graduate research fellowship to University of Vermont Mechanical Engineering Ph.D. student Dan Orfeo from the Vermont Space Grant Consortium under NASA Cooperative Agreement NNX15AP86H helped with conducting the described experiments. Additionally, some of the components for the OAM testbed came from a U.S. Army SBIR Phase II award, entitled “Multi-static Ground Penetrating Radar for Buried Explosive Hazard Detection” with White River Technologies, Contract Number W909MY-17-C-0020.

PARTICIPANTS:

Participant Type: PD/PI
Participant: Dryver R Huston
Person Months Worked: 1.00 **Funding Support:**
Project Contribution:
International Collaboration:
International Travel:
National Academy Member: N
Other Collaborators:

Participant Type: Co PD/PI
Participant: Tian Xia
Person Months Worked: 1.00 **Funding Support:**
Project Contribution:
International Collaboration:
International Travel:
National Academy Member: N
Other Collaborators:

RPPR Final Report
as of 14-Nov-2019

CONFERENCE PAPERS:

Publication Type: Conference Paper or Presentation **Publication Status:** 1-Published
Conference Name: Detection and Sensing of Mines, Explosive Objects, and Obscured Targets XXIV
Date Received: 11-Sep-2019 Conference Date: 14-Apr-2019 Date Published:
Conference Location: Baltimore, United States
Paper Title: Orbital angular momentum assisted ground penetrating radar
Authors: Daniel Orfeo, Wilson Ezequelle, Tian Xia, Dryver Huston
Acknowledged Federal Support: **Y**

Publication Type: Conference Paper or Presentation **Publication Status:** 2-Awaiting Publicat
Conference Name: IEEE 2019 IEEE International Symposium on Phased Array Systems and Technology
Date Received: 11-Sep-2019 Conference Date: 15-Oct-2019 Date Published: 15-Oct-2019
Conference Location: Waltham, MA
Paper Title: Phased Array for Control of Orbital Angular Momentum in Microwave Systems
Authors: Daniel Orfeo, Dylan Burns, Tian Xia, Dryver Huston
Acknowledged Federal Support: **Y**

REPORT DOCUMENTATION PAGE

Form Approved
OMB No. 0704-0188

1. REPORT DATE *(DD-MM-YYYY)*	2. REPORT TYPE	3. DATES COVERED *(From - To)*
	Final Performance Report	12 June 2018 to 11 June 2019

4. TITLE AND SUBTITLE
OAM and Quantum Penetrating Radar

5a. CONTRACT NUMBER
W911NF1810193

5b. GRANT NUMBER

5c. PROGRAM ELEMENT NUMBER

6. AUTHOR(S)
Dryver R. Huston, Tian Xia

5d. PROJECT NUMBER

5e. TASK NUMBER

5f. WORK UNIT NUMBER

7. PERFORMING ORGANIZATION NAME(S) AND ADDRESS(ES)
University of Vermont & State Agricultural College
85 S Prospect St.
Burlington, VT 05405-0170

8. PERFORMING ORGANIZATION REPORT NUMBER

9. SPONSORING/MONITORING AGENCY NAME(S) AND ADDRESS(ES)
US Army ACC-APG-RTP W911NF
800 Park Office Drive, Suite 4229
Research Triangle Park, NC 27709

10. SPONSOR/MONITOR'S ACRONYM(S)
DURIP

11. SPONSOR/MONITOR'S REPORT NUMBER(S)

12. DISTRIBUTION/AVAILABILITY STATEMENT
Unclassified Unlimited

13. SUPPLEMENTARY NOTES

14. ABSTRACT

This project acquired and assembled equipment for an experimental test bed for research into digital control, orbital angular momentum (OAM) synthesis and reception, and the possible exploitation of quantum effects in penetrating radars. The acquisition included a PXIe-based microwave transceiver with 4 channels of digitally-controlled output tightly synchronized with 4 channels of digital data acquisition and 1 GHz 1 GHz baseband, a 500 MHz bandwidth and FPGA programmability; a pair of 6 GHz RF Vector Signal generators; and testbed accessories. A first round of the tests produced results consistent with the generation and reception of vortex-shaped OAM microwave waveforms with phased antenna arrays.

15. SUBJECT TERMS
orbital angular momentum, microwave, ground penetrating radar, quantum sensing

16. SECURITY CLASSIFICATION OF:			17. LIMITATION OF ABSTRACT	18. NUMBER OF PAGES	19a. NAME OF RESPONSIBLE PERSON
a. REPORT	b. ABSTRACT	c. THIS PAGE	SAR		Dryver R. Huston
					19b. TELEPHONE NUMBER *(Include area code)* 802-656-1922

Table of Contents

1. Project Summary

The goal of this project was to acquire microwave test equipment and to assemble a test bed to enable research into high-performance ground and wall penetrating radars and related topics. The emphasis is on the use of digital control, orbital angular momentum (OAM) control and the exploitation of quantum effects.

Three primary pieces of equipment along with accessories supporting the assembly of an experimental testbed were acquired. The first piece of equipment is a PXIe-based digitally controlled and programmable microwave transceiver. The unit has 4 channels of output tightly synchronized with 4 channels of input, with 1 GHz baseband, and 500 MHz bandwidth. The two additional pieces of equipment are a pair of 6 GHz RF Vector Signal generators. Additional items include custom waveguides and couplers to support the control, routing and mixing of microwave signals. Due to improved pricing from the vendor, this configuration is more capable that that originally proposed.

Five anticipated uses of the equipment are: 1. A system to support research into the digital control of time and frequency content of classical penetrating radar systems. This includes multi-static and phased array configurations, time and frequency domain compressive radar sensing, and software defined cognitive penetrating radar systems. 2. A system to support research into the use of controlled OAM microwaves, along with related quantum effects to improve the performance of penetrating radars. 3. A testbed for applied problems that can benefit from controlled OAM microwave radars including the location and classification of buried objects, determining the structural characteristics of walls, locating objects behind walls, operating orthogonal antenna arrays, and the operation of penetrating radars in electromagnetically challenging environments. 4. A testbed for related microwave research, such as software-defined radio communications. 5. Serve as an educational tool for students working in areas of microwave engineering, sensing, cognitive systems and structural identification.

A first round of the tests produced results consistent with the generation and reception of vortex-shaped OAM microwave waveforms with phased antenna arrays. Subsequent testing with a beamline obstruction found a test configuration where a vortex beam with OAM produced larger signals than an equivalent beam without OAM. This result, while intriguing, requires more investigation and confirmation of the repeatability and scope of the effect.

2. Description of Proposed Equipment Acquisition

The following is a brief description of the equipment originally proposed for acquisition.

The first piece of equipment was a PXIe-based time-domain-synchronized 2-input 2-output microwave transmit/receive system, along with a 3 GHz RF Vector Signal generator. This system has four main components: 1. A PXIe 18-slot 24GB/s instrument rack that houses instrument

modules for the rest of the system. The rack and modules contain an onboard PC controller and provide a custom instrument control programming environment. The availability of extra memory slots allows for expansion to add more modules. 2. A Two-Channel 1 GSPS 14-bit PXI Arbitrary Waveform Generator. 3. A Two Channel, 14-bit, 500 MHz GS/s PXIe Digitizer. And 4. MXG X-Series RF Vector Signal Generator. Some details are:

1. **PXIe 10-slot 8GB/s Instrument Rack:**
   a. **PXIe Chassis:** PXIe Chassis 10-slot, 3U, 24GB/s (Keysight M9019A $4,226); b. PXIe Embedded Controller: with Intel i7, 4 GB RAM, 240 GB SSD, Windows Embedded Standard 7 (64 bit), Memory, 16GB (Keysight M9037A $6,898), c. HVI Programming Environment (Keysight M3601A $1,692), and d. Graphical FPGA Design Environment (Keysight M3602A $2,542); Total ($15,358).
   b. **PXI Arbitrary Waveform Generator:** Two channel 1 GSPS, 14 bits with Dual modulation capability (amplitude and angle), Enabled FPGA programming, Enabled HVI programming, Variable sampling clock, Xilinx FPGA, 2 GB Memory, (Keysight M3202A $16,483).
   c. **PXIe Digitizer:** Two Channel, 14-bit, DC Coupled, 500 MHz bandwidth, Memory, 2GB, with HVI and FPGA programmability (Keysight M9203A $0 special discount).
2. **MXG X-Series RF Vector Signal Generator:** Two channel, LO in/out for phase coherency, High output power, Multifunction generator, Frequency range, 9 kHz to 3 GHz, ARB baseband generator (80 MHz RF bandwidth, baseband generator with real-time capability, AM, FM, phase modulation, Narrow pulse modulation, Enhanced low phase noise (Keysight N5182B $64,376)
3. **Total Price: $96,216**

In addition to the above equipment, it was proposed to acquire accessories to support these instruments, including custom-machined waveplates and antennas for generating and receiving microwaves photons with controlled OAM, and leading to experiments based on electromagnetic wave shape control, hyperentanglement and frequency-domain entanglement. The funding for supplies in the amount of $1,333 was for the purchase of microwave cables, probes, mixers, absorbing foam and switches to support using the test equipment.

3. Description of Equipment Purchased

The following is a brief description of the equipment purchased as part of this project. The acquired equipment was similar to the proposed configuration but differed in performance specifications, number of items and testbed configuration. This included a 4-channel arbitrary waveform generator source instead of the original 2-channel version, and an increase in the frequency range of the RF Vector Signal Generators from 3 GHz to 6 GHz to provide better support for making microwaves with OAM using phased array methods, instead of the originally proposed wave plates. Better pricing from the vendor was the primary reason for the difference. The purchased equipment items appear in Figure 1. Details follow:

1. **PXIe 10-slot 8GB/s Instrument Rack and Modules:**
   a. **PXIe Chassis** PXIe Chassis 10-slot, 3U, 24GB/s (Keysight M9019A $4,418.11); b. PXIe Embedded Controller: with Intel i7, 4 GB RAM, 240 GB SSD, Windows Embedded Standard 7 (64 bit), Memory, 16GB (Keysight M9037A $7,207.67), c. HVI Programming Environment (Keysight M3601A $1,768.00), and d. Graphical FPGA Design Environment (Keysight M3602A $2,656.25); Total ($16,050.03).
   b. **PXI Arbitrary Waveform Generator:** Four channel 1 GSPS, 14 bits with Dual modulation capability (amplitude and angle), Enabled FPGA programming, Enabled HVI programming, Variable sampling clock, FPGA, Xilinx, Memory, 2 GB, (Keysight M3202A $17,300.90).
   c. **PXIe Digitizer:** Four Channel, 14-bit, DC Coupled, 500 MHz bandwidth, 2 GB Memory, with HVI and FPGA programmability (Keysight M3102A $0 special discount).
2. **MXG X-Series RF Vector Signal Generators:** Two units, LO in/out for phase coherency, High output power, Multifunction generator, Frequency range, 9 kHz to 6 GHz, ARB baseband generator (80 MHz RF bandwidth, baseband generator with real-time capability, AM, FM, phase modulation, Narrow pulse modulation, Enhanced low phase noise (Keysight N5182B $62,467.50)
3. **Total Price: $95,818.43**

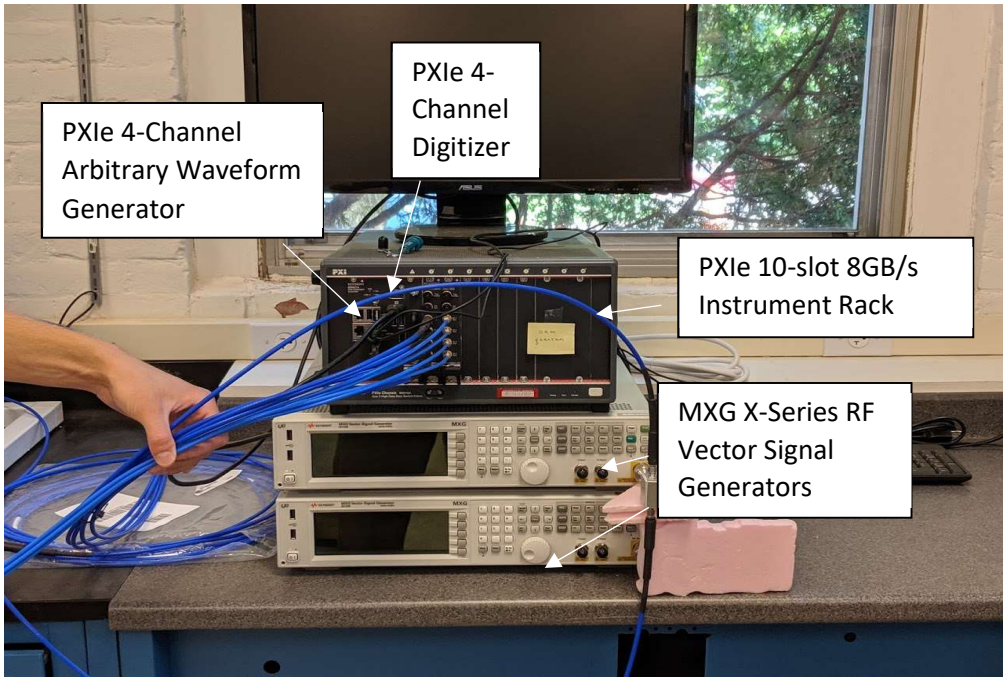

Figure 1 Equipment acquired including: PXIe 10 slot 8GB/s instrument rack, PXIe 4-channel arbitrary waveform generator with 1 GSPS and 14 bits resolution, PXIe 4-channel digitizer with 500 MHz bandwidth and 14-bit resolution, 2 MXG X-Series RF Vector Signal Generators with 9 kHz to 6 GHz frequency range and FPGA programmable ARB baseband generator with 80 MHz RF bandwidth.

In addition to the equipment a set of supplies in the form of cables, splitters, phase shifters, mixers, antennas and lumber for the purpose of setting up a testbed for the generation and reception of OAM waves. This is a 4-channel send to 4-channel receive system. Figure 2 is a picture of the testbed. Figure 3 is a schematic diagram of the testbed system.

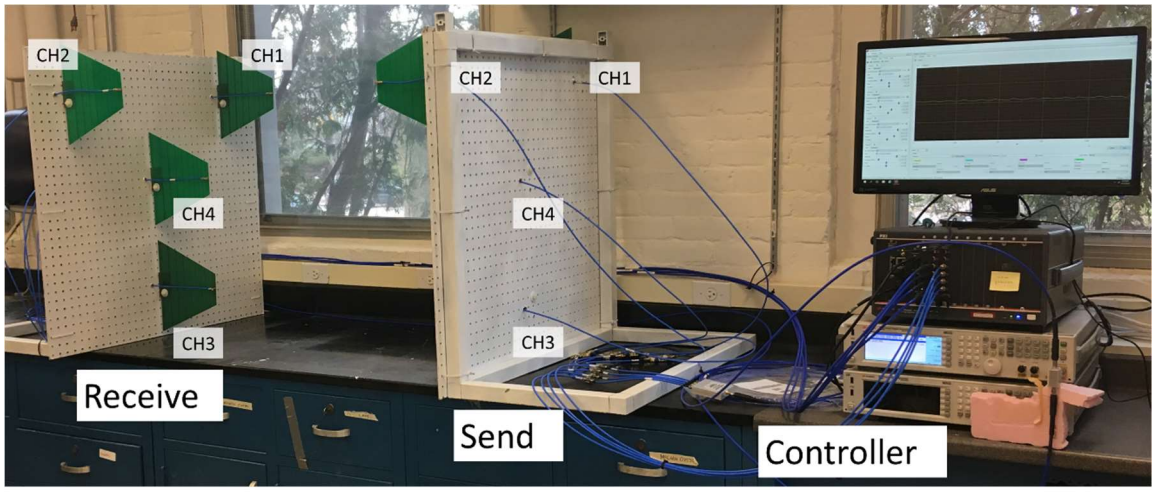

Figure 2 4-Channel in to 4-Channel out OAM testbed

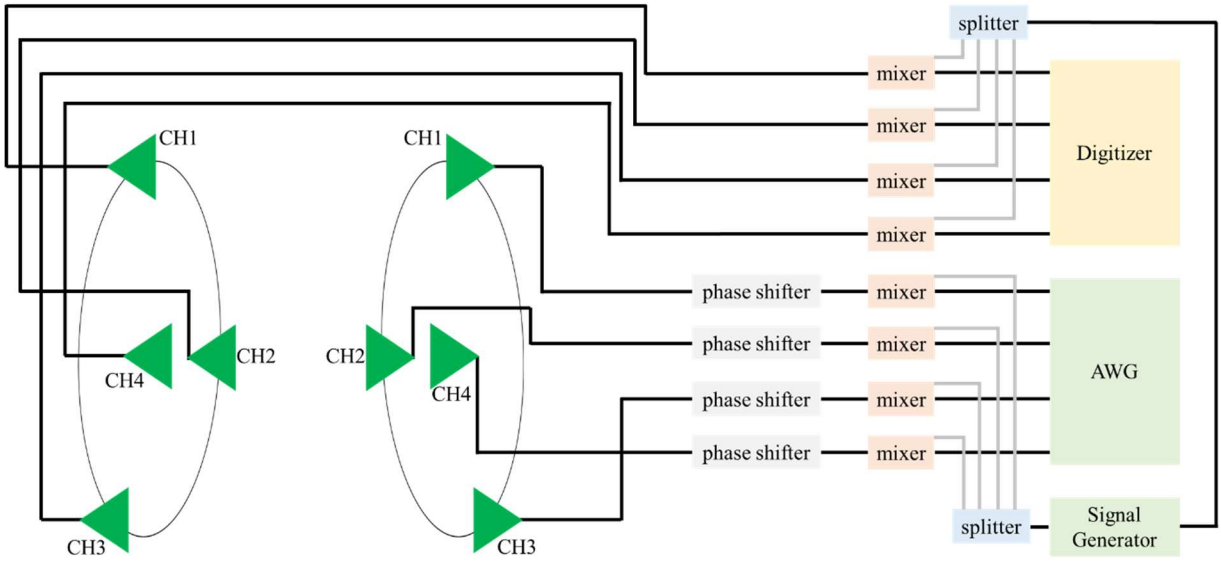

Figure 3 Schematic diagram of 4-channel send to 4-channel receive OAM testbed

The testbed has the following features:

1. Location on the same PXIe bus synchronizes the 4-channel source and 4-channel receiver/digitizer to run on the same clock. This minimizes noise due to jitter and timing drift.
2. The antennas are log period PCB boards from Kent Electronics (Model LP0410) with a 400 MHz to 1 GHz bandwidth at 5-6dBi Gain. The far-field electric polarization is parallel to the plane of the board.
3. The pegboard construction allows for rapid reconfiguration of geometry and polarization.

4. Background and Motivation

The motivation for acquiring this equipment and assembling the associated experimental testbed is for research that advances the state of the art and fundamental understanding of penetrating radar systems. The anticipated research includes extending the performance of penetrating radars to operate in challenging conditions, such as limited penetration depth due to adverse soil conditions, obscure targets and cluttered subsurface conditions. Potential applications include detection of landmines, IEDs, covert tunnels, human presence inside of buildings, fire location, underground infrastructure location and classification – especially in cluttered urban environments, identification of structural configuration of buildings, and operation with low levels of emitted radiation. Three main research thrusts are: 1. Agile time and frequency control with classical radar methods; 2. Active shape control of emitted waves, including vorticity, i.e. Orbital Angular Momentum (OAM); and 3. Quantum effects.

4.1 Classical Ground Penetrating Radar Systems

Ground penetrating radar (GPR) and wall penetrating radars operate by launching, receiving and analyzing electromagnetic (EM) waves that interact with subsurface features in dielectric structures, such as the earth, concrete structures and building walls. The present state-of-the-art is that GPR is a mature technology that continues to improve in capabilities, yet still has significant performance limitations due to attenuation in lossy media, scattering in heterogeneous media, clutter and resolution of complicated geometries. The primary interactions rely on the spatially varying dielectric properties of structural material to reflect, scatter and absorb electromagnetic waves. Each of these interactions depends on the interplay of wavelength, polarization, and the geometric distribution of dielectric parameters. An example appears in Figure 4 where the relative direction of linear polarization has a dramatic effect on the ability to resolve steel reinforcing bars in a concrete slab. Strong reflections occur when the polarization of the $\vec{E}$ field aligns with the conductive path of the reinforcing bar as the antenna passes over the slab in a transverse direction. The B-scans show the rebar reflections as hyperbolas due to the geometric nonlinearity of off-axis reflections.

The results in Figure 4 show that subsurface imaging performance can depend on geometric properties of the propagating field, such as polarization. Developments over the past two decades indicate that other controls over the geometry of the propagating waves are possible, including those with OAM vorticity.

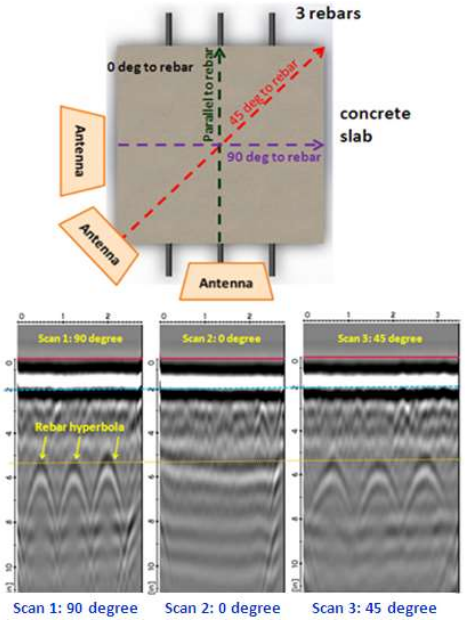

Figure 4 Effect of linear polarization direction on B-scans and the ability to detect steel reinforcing bars in concrete

4.2 Orbital Angular Momentum

EM beams are collections of waves of field disturbances that travel in the same direction, centered on an axis. Figure 2 shows a generic beam propagating along the z-axis. Most penetrating radars use EM beams to probe subsurface features. Electromagnetic waves and the photons that comprise the waves can carry both linear and angular momentum. The angular momentum can appear as either spin or orbital. Spin angular momentum (SAM) corresponds to polarization, whereas orbital angular momentum (OAM) corresponds to wave vorticity.

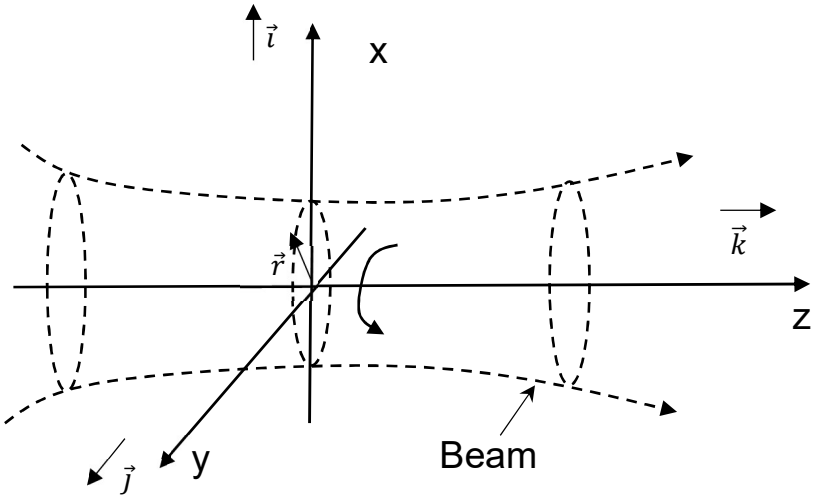

Figure 2. Electromagnetic beam centered on and propagating along z-axis with possible rotation component

In classical physics, the principal EM vector fields are the electric field $\vec{E}$, and the magnetic field, $\vec{B}$. When disturbed these fields will transmit the disturbance through space and time in a manner described by Maxwell's equations [Wangsness, 1986].

$$\nabla \times \vec{\mathrm{B}} = \frac{1}{\mathrm{c}^2}\frac{\partial \vec{\mathrm{E}}}{\partial \mathrm{t}} \tag{1}$$

$$\nabla \times \vec{\mathrm{E}} = -\frac{\partial \vec{\mathrm{B}}}{\partial \mathrm{t}} \tag{2}$$

$$\nabla \cdot \vec{\mathrm{B}} = 0 \tag{3}$$

$$\nabla \cdot \vec{\mathrm{E}} = 0 \tag{4}$$

In a vacuum, or air at most wavelengths and power levels, ϵ_0 = 8.854 x 10-12 farad/m, μ_0 = 4π x 10-^{7} N/A2 and c = 2.998 x 10^8 m/s. Combining the curl of (1) and (2) with (3) and (4), and using the following identity for an arbitrary continuous vector field $\vec{A}$

$$\nabla \times \nabla \times \vec{\mathrm{A}} = \nabla\nabla \cdot \vec{\mathrm{A}} - \nabla^2 \vec{\mathrm{A}} \tag{5}$$

leads to the following vector wave equations and that describes the propagation of electric and magnetic field vectors

$$\nabla^2 \vec{\mathrm{E}} = \frac{1}{\mathrm{c}^2}\frac{\partial^2 \vec{\mathrm{E}}}{\partial \mathrm{t}^2} \tag{6}$$

$$\nabla^2 \vec{\mathrm{B}} = \frac{1}{\mathrm{c}^2}\frac{\partial^2 \vec{\mathrm{B}}}{\partial \mathrm{t}^2} \tag{7}$$

c is the wave speed.

Scalar waves describe many properties of corresponding vector waves and provide a guide to approximate solutions, including descriptions of propagating beams [Saleh 1991]. The scalar wave equation is

$$\nabla^2 \psi = \frac{1}{\mathrm{c}^2}\frac{\partial^2 \psi}{\partial \mathrm{t}^2} \tag{8}$$

A useful property of monochromatic scalar waves is that they propagate at a constant frequency. This leads to a form that separates into a product of spatial and temporal terms

$$\psi(x, y, z, t) = \varphi(x, y, z)e^{i\omega t} \tag{9}$$

Substitution into the wave equation (8) produces a scalar Helmholtz equation for the spatial term

$$\nabla^2\varphi + k^2\varphi = 0 \tag{10}$$

Solutions to this Helmholtz equation are the spatial envelopes of oscillating waves. The individual components of the $\vec{E}$ and $\vec{B}$ fields in propagating EM waves satisfy the Helmholtz equation, but are also collectively constrained by Maxwell's equations. Possible solutions include plane waves and beams.

Durnin [1987] demonstrated the existence of a class of beams derived from the scalar wave equation with intensity distributions that do not change with propagation. Theses beams, known as diffraction-free or propagation-invariant beams, have the general form

$$\mathrm{E}(\mathrm{x}, \mathrm{y}, \mathrm{z} \geq 0, \mathrm{t}) = \exp[\mathrm{i}(\beta\mathrm{z} - \omega\mathrm{t})] \int_0^{2\pi} \mathrm{A}(\varphi)\exp[\mathrm{i}\alpha(\mathrm{x}\cos\varphi + \mathrm{y}\sin\varphi)]\mathrm{d}\varphi \tag{11}$$

with the constraint

$$\beta^2 + \alpha^2 = \left(\frac{\omega}{\mathrm{c}}\right)^2 \tag{12}$$

A(φ) is an arbitrary complex integrable function. Direct substitution of the diffraction-free beam, (15) into (14) verifies that it is a solution to the Helmholtz equation. A simplification is to set A(φ) to a constant, which leads to circular symmetry and a subset of solutions, known as Bessel beams, with field $\mathrm{E_B}$ given as

$$\mathrm{E_B}(\mathrm{x}, \mathrm{y}, \mathrm{z} \geq 0, \mathrm{t}) = \exp[\mathrm{i}(\beta\mathrm{z} - \omega\mathrm{t})] \int_0^{2\pi} \exp[\mathrm{i}\alpha(\mathrm{x}\cos\varphi + \mathrm{y}\sin\varphi)]\mathrm{d}\varphi \tag{13}$$

and

$$\mathrm{E_B}(\mathrm{x}, \mathrm{y}, \mathrm{z} \geq 0, \mathrm{t}) = \exp[\mathrm{i}(\beta\mathrm{z} - \omega\mathrm{t})]\mathrm{J}_0(\alpha\mathrm{R}) \tag{14}$$

J_0 is a Bessel function of the first kind of zero order. These beams, known as Bessel beams, have an intensity distribution that varies in the lateral direction, but is invariant with respect $\mathrm{I_B}$,

$$\mathrm{I_B} = \frac{1}{2}|\mathrm{J}_0(\alpha\mathrm{R})|^2 \tag{15}$$

If α= 0, then $J_0(\alpha R) = 1$, and the Bessel beam reverts to the special case of a plane wave. Similar to plane waves Bessel beams are physically unrealizable due to the infinite lateral extent with a slow dropoff in amplitude leading to infinite total energy. Bessel beams have a noteworthy self-healing property in that partial blockages and obstructions produce shadows that disappear with propagation distance due to a self-compensating diffraction effect.

The paraxial wave equation is a useful approximation to the Helmholtz equation. It applies to elongated monochromatic beams. The key to the approximation is that elongation leads to small spatial gradients with respect to the propagation axis. This leads to a spatial form as the product of a slowly-varying 3-D scalar function A(x,y,z) plane wave propagating in the z-direction where

$$\varphi(x,y,z) = A(x,y,z)e^{-ikz} \tag{16}$$

with A(x,y,z) varying slowly compared with the wavelength. The paraxial wave equation becomes

$$\frac{\partial^2 A}{\partial x^2} + \frac{\partial^2 A}{\partial y^2} - i2k\frac{\partial A}{\partial z} = 0 \tag{17}$$

It is of interest to note that (16) is in the form of a Schrödinger equation.

The Gauss-LaGuerre (GL) modes are a set of solutions to the paraxial equation for beams with circular symmetries. In cylindrical coordinates the GL modes $\mathrm{A_{GL}(r,\theta,z)}$ are

$$\begin{aligned}\mathrm{A_{GL}(r,\theta,z)} = &\frac{\mathrm{C}}{\left(1+\frac{\mathrm{z}^2}{\mathrm{z_R^2}}\right)^{\frac{1}{2}}}\left(\frac{\mathrm{r}\sqrt{2}}{\mathrm{w(z)}}\right)^{l}\mathrm{L_G^l}\left(\frac{2\mathrm{r}^2}{\mathrm{w}^2\mathrm{(z)}}\right)\\ &\times\exp\left(\frac{-\mathrm{r}^2}{\mathrm{w}^2\mathrm{(z)}}\right)\exp\left(\frac{-\mathrm{ikr}^2\mathrm{z}}{2(\mathrm{z}^2+\mathrm{z_R^2})}\right)\exp(-\mathrm{i}l\theta)\\ &\times\exp\left(\mathrm{i}(2\mathrm{p}+l+1)\mathrm{atan}\left(\frac{\mathrm{z}}{\mathrm{z_R}}\right)\right)\end{aligned} \tag{18}$$

with z_R as the Raleigh range, w(z) as the beam radius, L_G^l as the associated Laguerre polynomial of order l and C is a constant [Allen 1992].

For Gauss-Laguerre beams based on the assumption of transverse $\vec{E}$ fields, the $\vec{B}$ fields produce a non-transverse component, leading to a helix. Integrating the angular momentum density of a beam made of a GL mode about the z-axis produces a non-zero angular momentum. The ratio of angular momentum L to linear momentum P in terms of the wavelength λ is

$$\frac{\mathrm{L}}{\mathrm{P}} = \frac{l\lambda}{2\pi} \tag{19}$$

Gauss-LaGuerre (GL) modes can produce EM beams with OAM. Each mode has a helical geometry, with the mode number corresponding to the number of intertwined helices [Yuan, 2017]. The GL modes are mutually orthogonal, when integrated over three spatial dimensions.

At the macroscopic wave scale OAM can be realized through the production of Gauss-LaGuerre (GL) modes. Each mode can be viewed as a helix, with the mode number corresponding to the number of intertwined helices, as shown in Figure 5 [Yuan, 2017]. At the photon scale, OAM appears as $lh/2\pi$ with l as an integer, and h as Planck's constant. Since the GL modes are mutually orthogonal and represent a means of propagating EM waves with different information content along the same beamline at the same wavelength. Cheng [2014] produced GL modes in 97 GHz microwaves using waveplates with spiral patterns of holes, Figure 6. In the optical regime Pu et al. [2015] used catenaries arranged in a spiral pattern for OAM control, Figure 7.

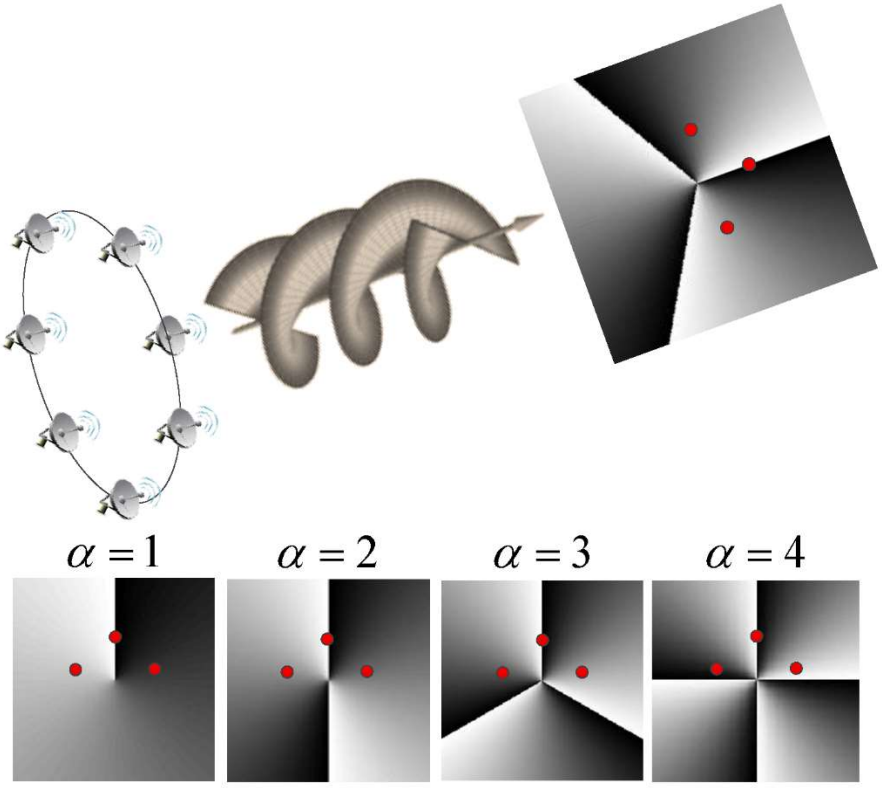

Figure 5 Propagating OAM, i.e. vortex, electromagnetic wave [Yuan 2017].

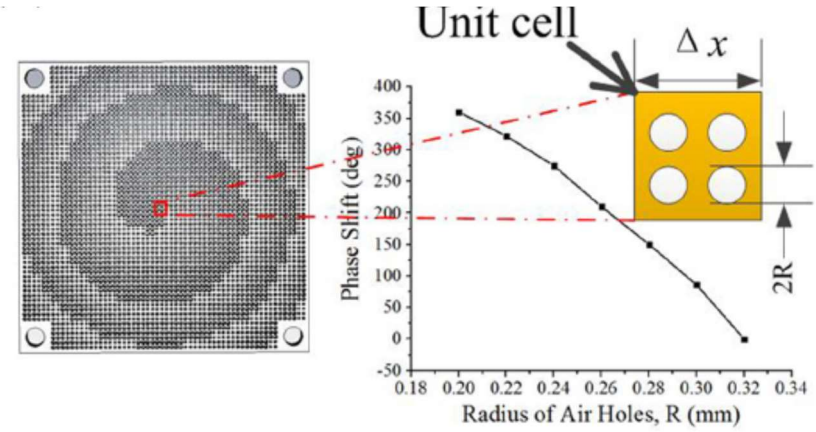

Figure 6 OAM waveplate for generating GL modes using a spiral array of holes [Cheng, 2014]

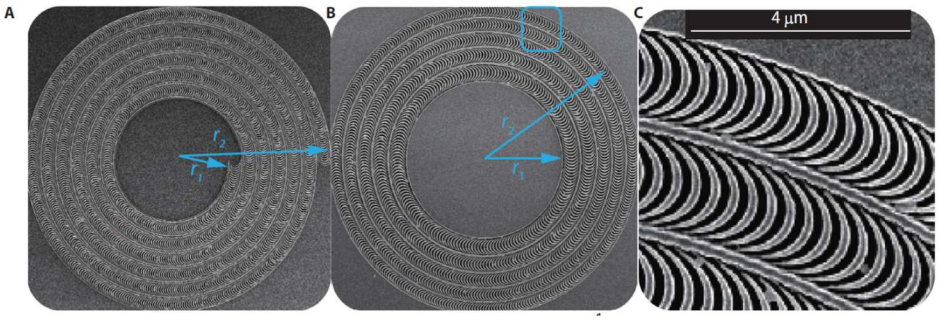

Figure 7 Spiral catenary array waveplates used to control OAM in optical EM waves [Pu, 2015]

A quantification of the linear and angular momentum of an electromagnetic field begins with the linear momentum density $\vec{g}$ of the field as determined by the Poynting vector $\vec{S}$ determines the linear momentum density as

$$\vec{g} = \epsilon_0 \vec{E} \times \vec{B} = \epsilon_0 \vec{S} \tag{20}$$

With a knowledge of the liner angular momentum, the orbital angular momentum density $\vec{L}$ is simply the moment of the linear momentum density $\vec{g}$ about a fixed reference point, determined as the cross product with position vector $\vec{r}$

$$\vec{L} = \vec{r} \times \vec{g} = \epsilon_0 \vec{r} \times \left(\vec{E} \times \vec{B}\right) = \epsilon_0 \vec{r} \times \vec{S} \tag{21}$$

Since this is analogous to the calculation of the angular momentum for a particle orbiting about a center, $\vec{L}$ is denoted as the Orbital Angular Momentum (OAM) of the field.

In an isotropic medium with monochromatic fields, the field disturbances oscillate at a single frequency ω, leading to the electric and magnetic field vectors being perpendicular, i.e. $\vec{E} \perp \vec{B}$. Monochromatic plane waves propagating in the z-direction at a frequency ω and wavenumber $k = \frac{\omega}{c}$ have uniform properties in the x- and y- directions with electric and magnetic fields

$$\vec{E} = \vec{E}_0 e^{i(kz-\omega t)} \tag{22}$$

$$\vec{B} = \vec{B}_0 e^{i(kz-\omega t)} \tag{23}$$

$\vec{E}_0$ and $\vec{B}_0$ are constant vectors, possibly complex, and parallel to the x-y plane and perpendicular to the direction of propagation, z. The momentum density is homogeneous for a plane wave. Integration of the z-component of the OAM density over an area in the x-y plane leads to zero total OAM for the plane wave.

4.3 Quantum OAM Effects

The quantum approach represents EM fields and waves as collections of photons. The quantum representation of linear momentum uses the operator $\hat{p}$ acting on position q as an observable and the states as eigenvalues of the operator, where

$$\hat{p} = -ih\nabla \tag{23}$$

For a photon, the linear momentum states are discrete integer multiples of the Plank constant $h = 2\pi\hbar$ with $\hbar$ = 1.054 x 10-34 J-s/rad. Taking the moment ($\vec{r} \times \hat{p}$) of the linear momentum operator produces an angular momentum operator $\hat{l}$. The possible states of angular momentum form two sets of discrete values [Messiah, 1965]. In both sets, the difference in angular momentum between states is integer multiples of $\hbar$. One set has multiples with the integers ...-2, -1, 0, 1, 2... The other set has half-integer multiples ...-3/2, -1/2, 1/2, 3/2... Isolated fermions, e.g. electrons, fall into the latter set with spin angular momentum (SAM) states of -1/2 and 1/2. Based on arguments of symmetry and invariance of the associated relativistic tensors, photons are bosons and fall into the former set with spin angular momentum states of -1 and 1 [Pauli 1940]. In addition to spin, photons have orbital angular momentum state components that are also integers. It may remain an open question as to whether it is possible in general to measure SAM and OAM as separable field components [Allen 1992].

4.4 Radars Based on Quantum Effects

Radar systems that take advantage of the peculiar nature of quantum effects hold the potential to provide superior sensing capabilities [Lanzagorta 2012]. Several distinct approaches, most based on entanglement and some based on quantized OAM, have been proposed:

Quantum illumination for enhanced sensitivity – Uses entangled photons for enhanced photodetection [Lloyd 2008] [Tan 2008] [Barzanjeh 2015]. The methods projects one set of photons onto the object under study and retains entangled complementary photons, i.e. ancilla, at the source. Photons reflected from the target combine with the entangled ancilla photons to produce an image, while rejecting unentangled photons. The result is enhanced sensitivity in presence of noise that is not possible with classical imaging systems.

Ghost imaging – Experiments in the optical domain using counting of photons with entangled OAM showed enhanced edge detection with phase differences that exceed classical correlations with violations of Bell's inequality [Jack, 2009].

Compressive sensing for quantum illumination – Compressive sensing is a technique that allows sensing of signals with sparse information content by undersampled measurements. Compressive sensing methods can be very effective in quantum illumination and imaging applications where using a dense of array of detectors is not practical [Howland, 2014].

Quantum interferometric sensing for enhanced depth of penetration – Allen [2008] patented a method for enhanced penetration and transmission of radar signals through lossy media with entangled photons. The concept begins with entangling groups of low-frequency, long-wavelength photons at the illumination source interfere upon return to provide the effective spatial resolution of high frequency short wavelength photons, but with the lower attenuation rates of low-frequency photons. These methods have been verified with experiments and can be further enhanced with adaptive optics [Lopaeva 2013] [Smith III JF. (2009)]

Hyperentanglement – Elementary objects, such as photons, possess multiple quantum degrees of freedom. It is possible to entangle some degrees of freedom while leaving others unentangled. This is known as hyperentanglement. An example is the quantized OAM of a photon. OAM degrees of freedom are distinct from the SAM of polarization and wavelength. Hyperentanglement has the potential for significantly increasing the performance of sensors by enhancing resolution, signal-to-noise ratios and measurement time [Smith, 2017]. Entanglement and OAM entanglement distillation with Hong-Ou-Mandel interference may be able to improve the identification of photons transmitted and received through atmospheric turbulence [Smith, 2009] [Ndagano, 2019].

Frequency-domain or wavelength entanglement – The generation and detection of individual sets of photons in the time domain can be challenging, especially for microwave frequencies. Frequency domain entanglement is a potentially viable workaround. It uses larger numbers of photons and entangles them by frequency content. Physical methods of generation include nonlinear frequency combs and ring resonators, optomechanical resonators, and molecular magnets [Mazeas 2016] [Andrews 2014] [Barzanjeh 2012] [Roslund 2014] [Xia 2015] [Cheng 2012].

Metamaterial entanglement – It is possible to use metamaterials to entangle the spin and orbital angular momentum of photons [Stay 2018]. The distinctive nature of photons and EM waves with different orbital angular momentum and vorticity allows for multiplexing multiple signals with the same frequency [Ren 2016]. Custom lasers with integrated spiral waveplates can produce visible laser beams with specified vorticity [Stellinga 2018].

Quantum Doppler sensing – It is possible to use quantum delay lines to implement quantum Doppler sensing for enhanced sensing in applications requiring low-level radiated emissions [Lanzagorta 2016].

5. Experiments Conducted with Acquired Equipment – Phased-Array Orbital Angular Momentum

A set of experiments using the newly acquired equipment an experimental testbed examined the viability of sending and receiving microwave beams containing controllable OAM at frequencies and dimensions comparable to those used in typical GPRs. Figure 1 Figure 2 shows the testbed. This is a phased-array system with a set of four send and of four receive linearly polarized antennas. Each set of four antennas lies in a plane with three of the antennas arranged in an equilateral triangle with side length of 0.8 m and the fourth antenna placed at the center of the triangle. The antennas have linear polarization and are mounted so as to allow manual adjustment of the polarization direction. The system uses a modular PXIe microwave transceiver system (Keysight M9037A) for digital control of the input and output using 50 MHz baseband signals mixed up to microwave frequencies and back to the baseband with an intermediate frequency (IF) of 750 MHz. Independent control is possible for each of the send channels. The transceiver synchronizes the timing of the source and receiver for minimization of phase jitter and drift.

5.1 Phased-Array OAM Source and Receive Experiments

The first experiments evaluated using the testbed as a phased-array for OAM beam source and reception. The rationale for the triangular antenna configuration is to use the three outer antennas (1, 2 and 3) to create a vortex through phase difference control and to use the center antenna (4) for an independent wave, possibly interfering with the other three in a ghost imaging application, Figure 8. The polarizations of all eight antennas are presently aligned in parallel with the intent of reducing polarization effects and leaving OAM effects as dominant. This system uses a baseband signal with e50 MHz center band, mixed with an RF signal of 750 MHz to produce and upconverted signal. It is the upconverted signal that is transmitted and received as an electromagnetic field disturbance through the free space between the antennas. Figure 9 shows a typical received signal in the upconverted state with the 50 MHz baseband producing a beating effect on the carrier IF of 750 MHz. The time histories shown in the subsequent figures are those that result from downconversion following reception by the receive antennas.

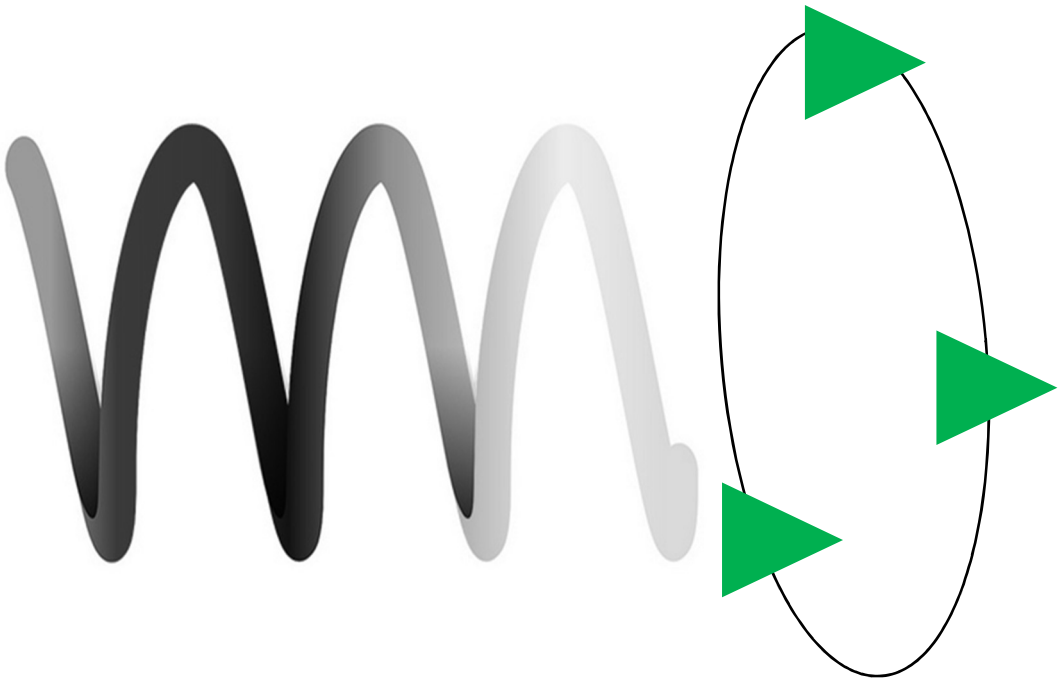

Figure 8 Three antenna array launching signals with same frequency and with 120º phase offset to produce and electromagnetic vortex.

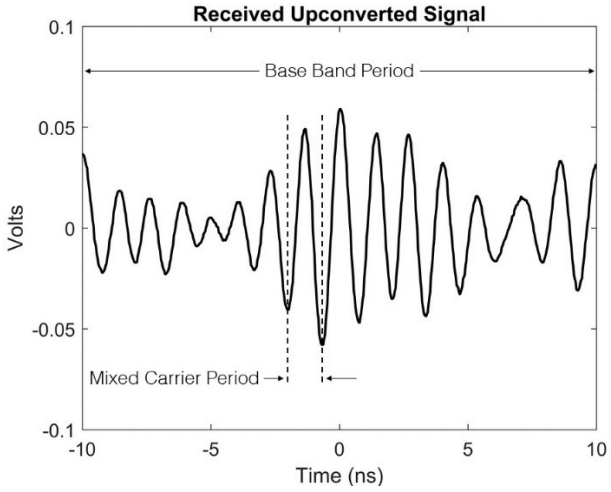

Figure 9 Typical mixed signal received at antenna containing both the baseband as a beating at 50 MHz and a faster IF band at 750 MHz

As a test of the phased array OAM technique, it is hypothesized that sending sinusoids at the same frequency, but with a 120 degrees relative phase offset out of channels 1, 2 and 3 will produce a beam that forms a vortex. Measuring this beam should produce sinusoids at receive channels 1, 2, and 3 with the same frequency and 120 degrees relative phase offset. Due to symmetry and equal amplitude superposition of channels 1, 2 and 3 a weak signal should appear at the center of the vortex with receive antenna 4. The results shown in Figure 6 confirm this hypothesis with

strong received signals in channels 1, 2 and 3 with 120 degrees offset and a weak signal at channel 4. A further test to confirm the vortex shape involved sliding the receive frame laterally so that receive antenna 4 aligns with the perimeter of the outer send antenna pattern. Figure 7 shows the results of this lateral move. Receive channel 4 is now positioned outside the center of the vortex and has a relatively strong amplitude. The next tests used the same setup as in Figures 4 and 6, but with an additional sinusoid at the same frequency driven out of the center channel 4. Figure 8 shows the addition of the center signal produces the same pattern in the outer channels 1, 2 and 3, but now with a stronger signal at the center channel 4.

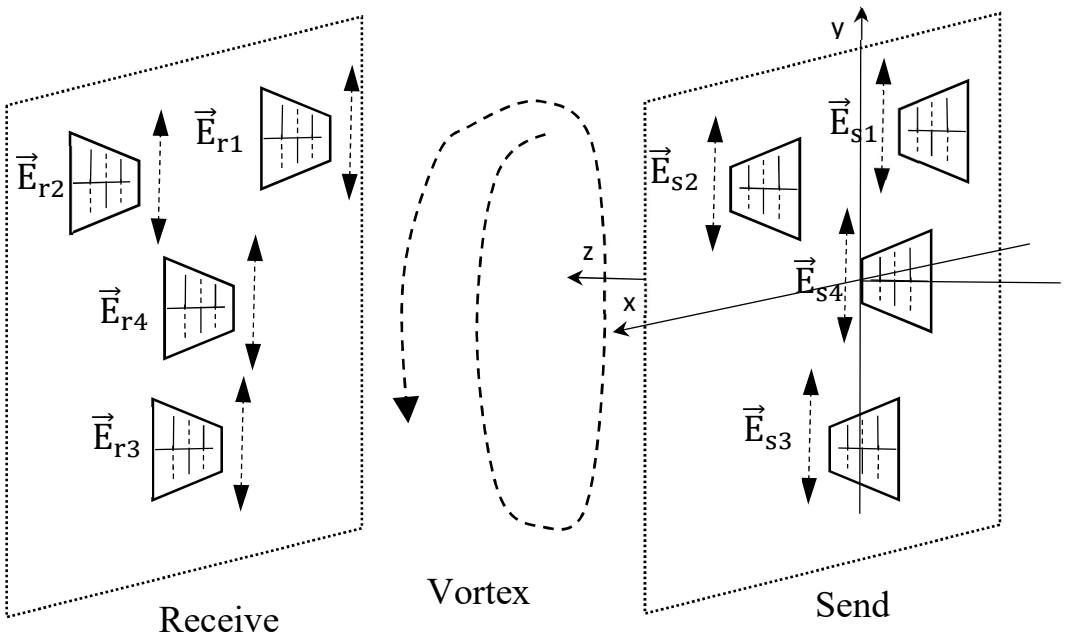

Figure 10 Antenna configuration with Cartesian coordinate system. Polarization indicated by dashed arrows. Vortex predicted to result from 120-degree phase offset from outer send antennas S1, S2 and S3.

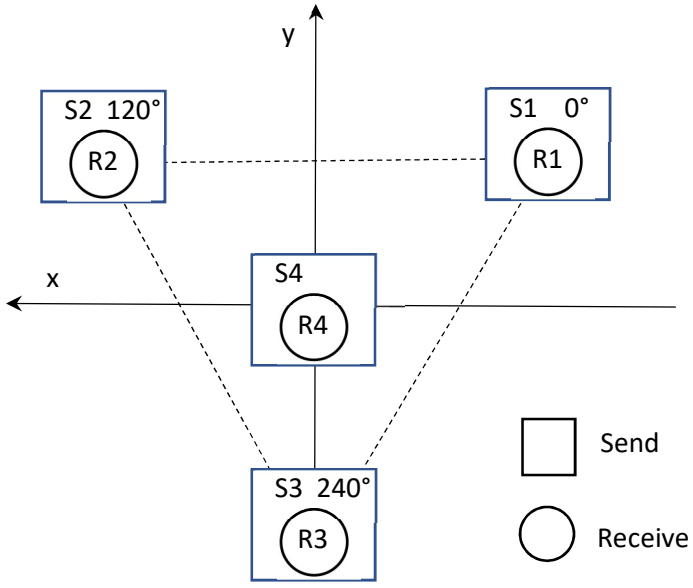

Figure 11 Beamline-axis view of source antennas, with listing of phase angle, and receive antennas. Both sets of antennas form equilateral triangle with center on beamline z-axis

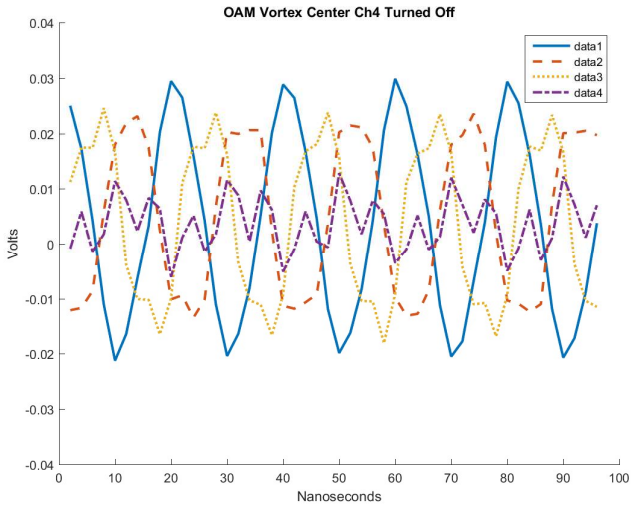

Figure 12 Received signals confirming formation of EM vortex using antenna configuration of Figure 11 with center send channel 4 off. Outer receive channels 1, 2 and 3 show 120 degree phasing and the center receive channel 4 has small amplitude, as predicted by the symmetry corresponding to a vortex.

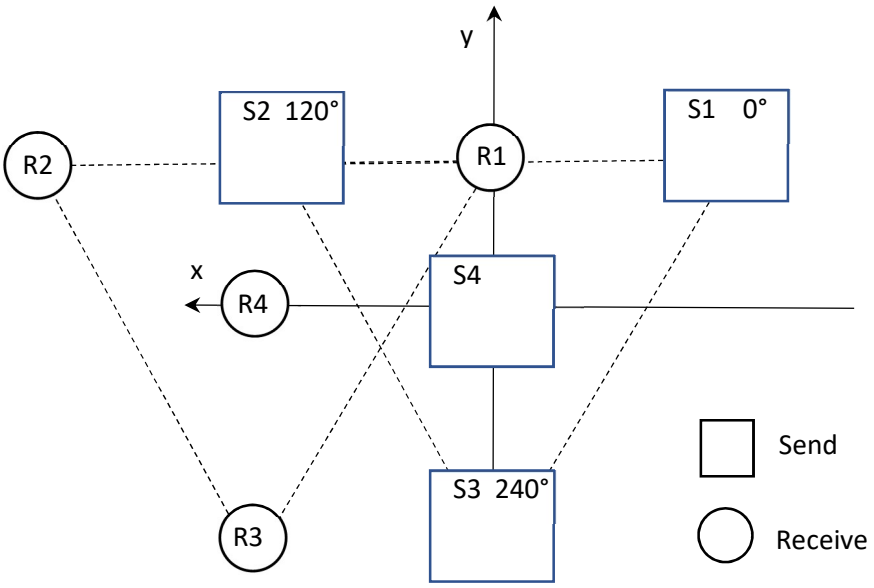

Figure 13 Beamline-axis view of source antennas with phase angle listed and receive antennas. Both sets of antennas form an equilateral triangle with send antennas centered on z-axis and receive antennas offset in the x-direction

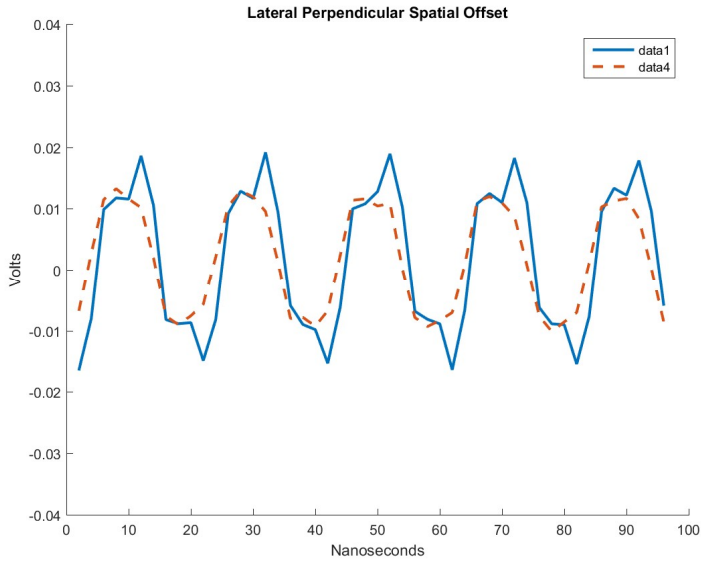

Figure 14 Lateral movement of receive array in x-direction, as shown in Figure 14. This moves center receive channel 4 to vortex perimeter which now picks up strong signal aligns with outer receive channel 1

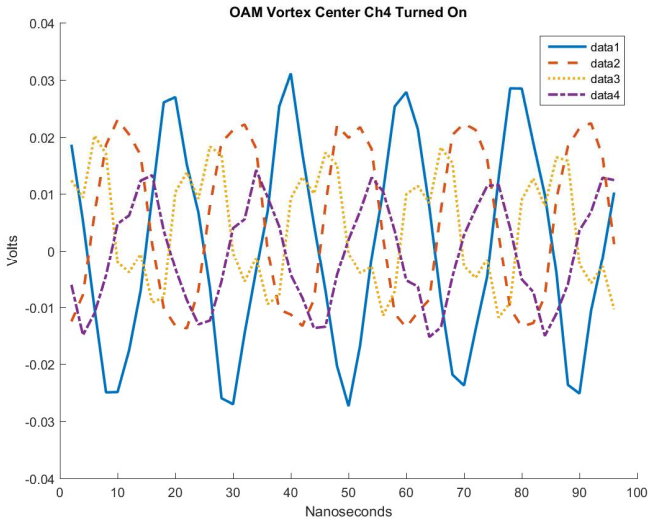

Figure 15 Received EM vortex with center send channel 4 on. Outer receive channels 1, 2 and 3 show 120-degree phasing and the center receive channel 4 has larger amplitude.

An additional evaluation of the testbed performance sent sinusoids with different frequencies of 40, 50 and 60 MHz out of channels 1, 2 and 3, respectively, using the configuration shown in Figure 16. The result was the reception of mixed, somewhat incoherent, beating signals, Figure 17.

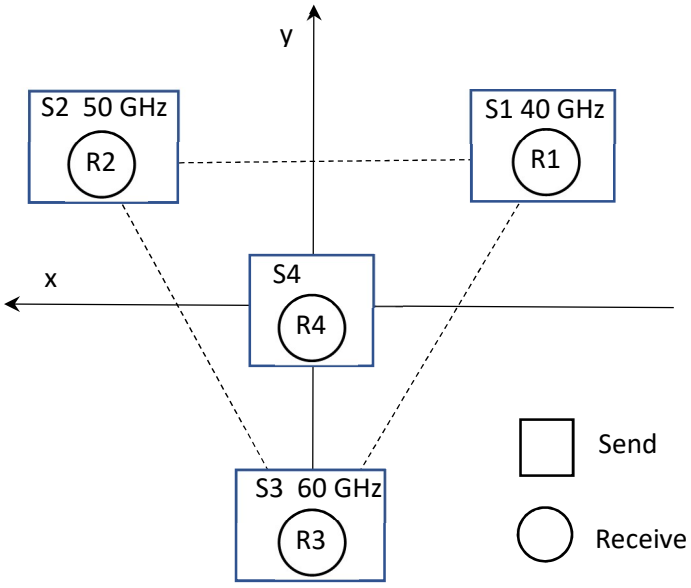

Figure 16 Beamline-axis view of source antennas, with listing of source signal frequency, and receive antennas. Both sets of antennas form equilateral triangle with center on z-axis.

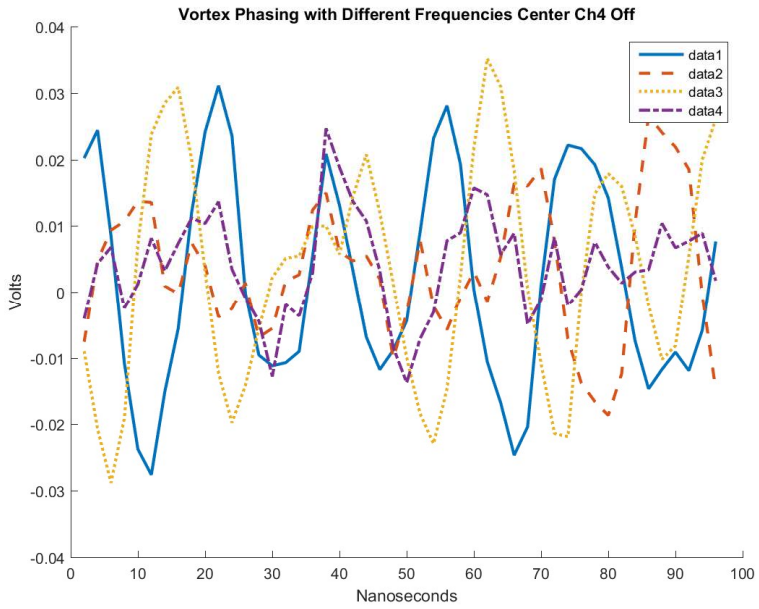

Figure 17 Sending of mixed frequencies with basebands of 40 MHz channel 1, 50 MHz channel 2 and 60 MHz channel 3 produce an incoherent beating signal at the receive antennas.

5.2 Obstruction and Recovery of Vortex OAM Beam

An interesting aspect about beams with OAM and circular symmetry is that a subset, i.e. the Bessel beams, have the capability to self-heal and reconstruct following an obstruction. It may be possible that other vortex beams possess similar capabilities. A simple set of preliminary experiments to explore this possibility follows.

Figure 18 shows the obstruction test setup in the OAM testbed. A conductive metal mesh screen provided an effective microwave obstruction. The first measurements used the source antennas to launch a vortex into a path that obstructs receive antennas 2, 3, and 4. Figure 19 shows a beamline view of the geometry. Figure 20 shows the received signals with unobstructed channel 1 picking up the strongest signal.

The second set of measurements used the source antennas launching waves in-phase in a non-vortex configuration. Figure 21 shows a beamline view of the geometry. Figure 22 shows the received signals. In this case the results differed from that of the vortex beam of Figure 20. For the in-phase beam, the received signal in unobstructed channel 1 was the same size as that of the obstructed channels 2, 3 and 4 and significantly smaller than that produced with the vortex beam in the same configuration. This is an intriguing result that hints at the possibility of reconstruction of waveforms following obstructions with vortex beams. Further testing is needed to confirm the repeatability and range of applicability of the results.

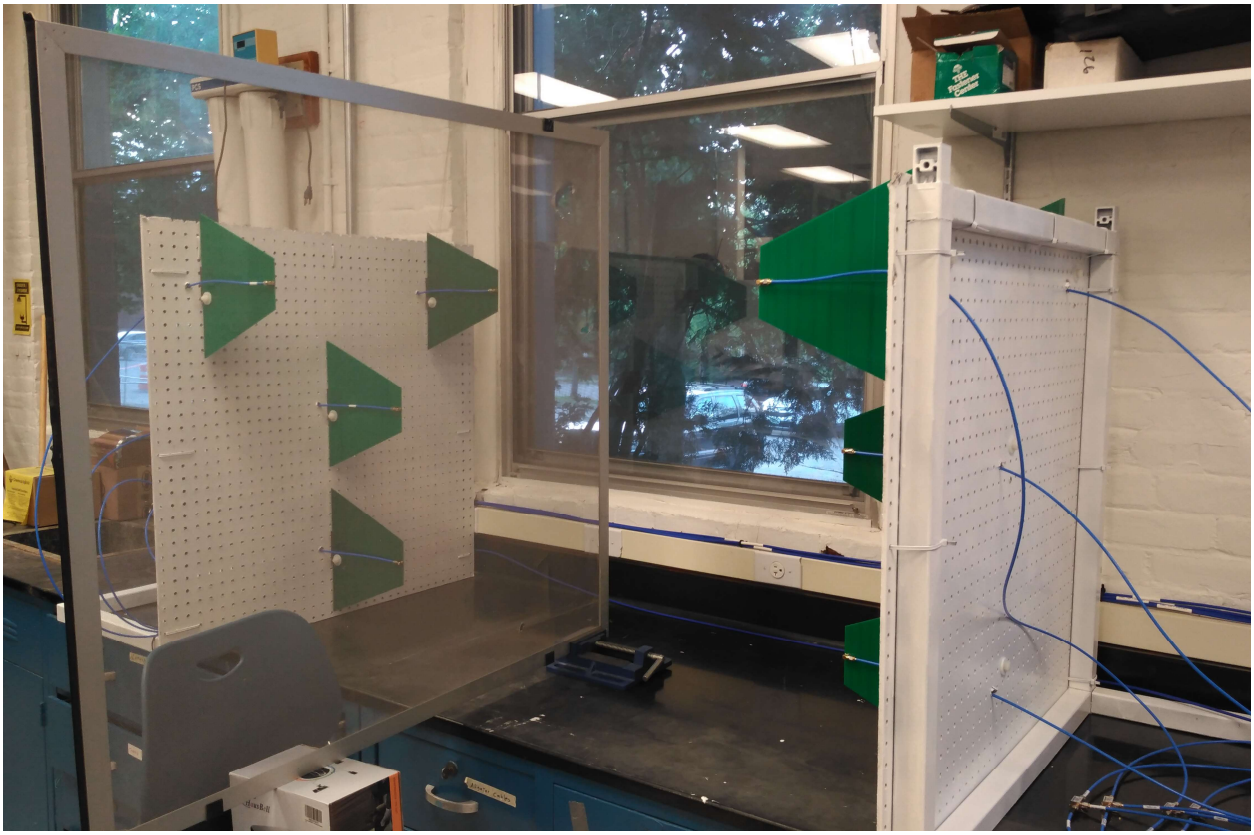

Figure 18 Conductive metal mesh screen serving as an obstruction in the beamline paths

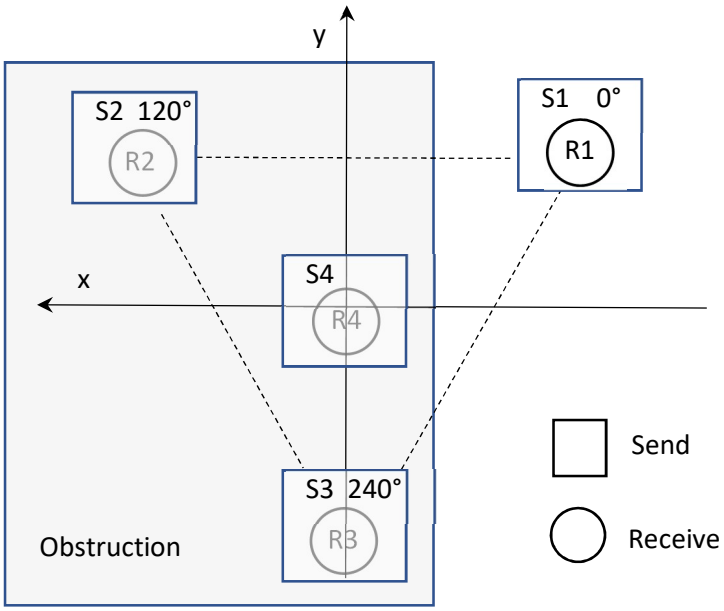

Figure 19 Beamline-axis view of obstruction recovery tests with vortex source. Shown are the antennas, with listing of phase angle received with no obstruction, and receive antennas. Both sets of antennas form equilateral triangle with center on z-axis. The electrically conductive obstruction blocks the direct path between the send and receive antennas 2, 3 and 4.

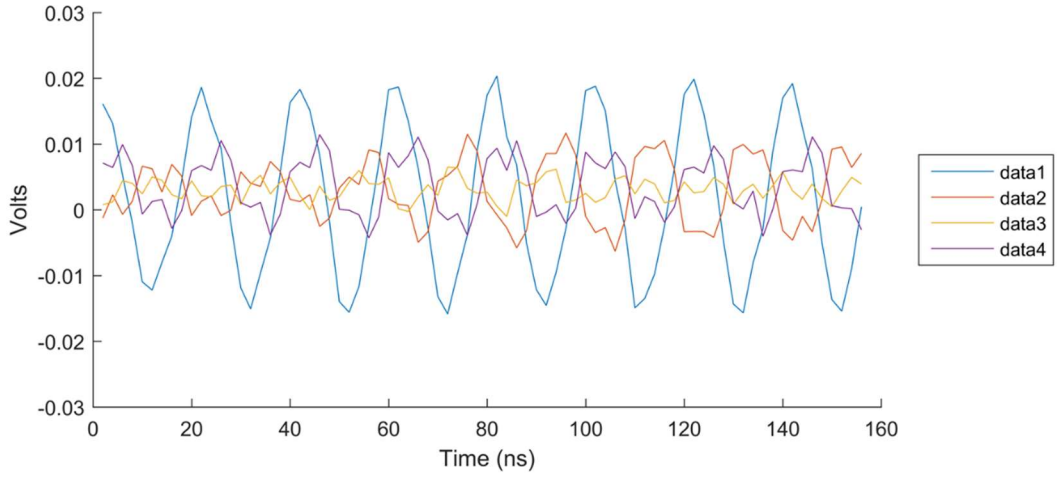

Figure 20 Received signals with vortex-shaped source and receive channels 2 and 3 blocked by conductive obstruction, with beamline geometry of Figure 19. Unobstructed receive channel 1 has the strongest signal.

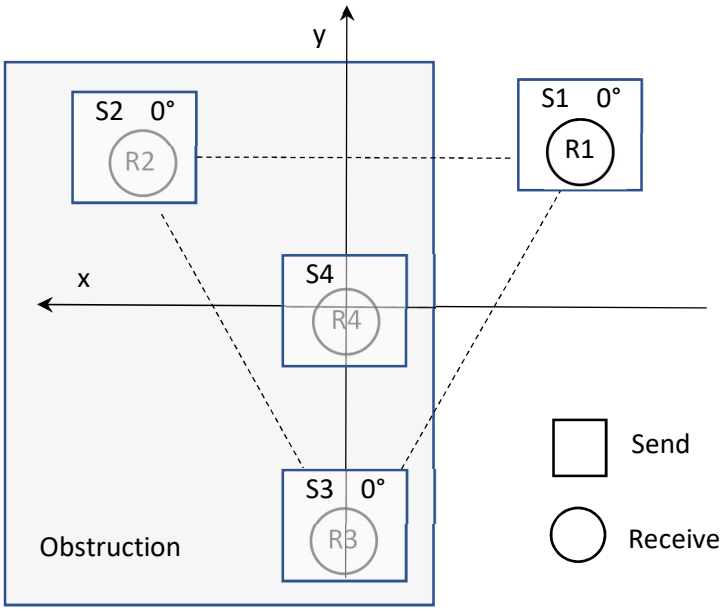

Figure 21 Beamline-axis view of obstruction recovery tests with all three source antennas in-phase. Shown are the antennas, with listing of phase angle received with no obstruction, and receive antennas. Both sets of antennas form equilateral triangle with center on z-axis. The electrically conductive obstruction blocks the direct path between the send and receive antennas 2, 3 and 4.

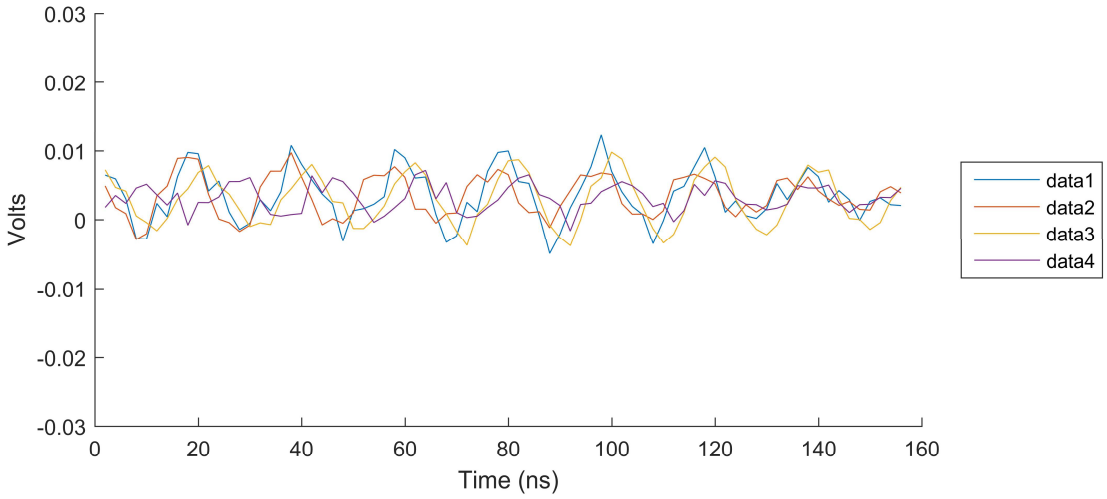

Figure 22 Received signals with three source antennas in phase and receive channels 2 and 3 blocked by conductive obstruction, with beamline geometry of Figure 21. The strength of the unobstructed receive channel 1 matches that of the obstructed channels 2 and 3.

6. Planned Possible Future Experiments

The test equipment and OAM testbed enable a series of possible future tests. The following is a listing of some of the possibilities.

6.1 Polarization v. OAM

The OAM testbed uses an array of log period PCB board antennas with a 400 MHz to 1 GHz bandwidth at 5-6 dBi Gain. The far-field electric polarization of these boards is parallel to the plane of the board. The nominal mode of operation of the OAM testbed is to generate signal waves in a 0-100 MHz baseband, mix them with a local oscillator signal of about 750 MHz to produce a signal in the range of about 850 MHz. This higher frequency upconverted signal forms the physical layer of the electromagnetic signal sent from the send antennas to the receive antennas. Electromagnetic vorticity involves OAM with integer values of angular momentum. Polarization involves SAM with -1/2 and 1/2 as values of angular momentum. Allen [1992] notes that it may not be possible to measure separately OAM and SAM (polarization) components. These experiments will investigate the effect of misaligning the polarization of send and receive antennas. The question to be explored is whether vorticity in the form of OAM has an influence on the sensitivity with respect to polarization. In a similar context, experiments with metamaterials indicate that it may be possible to entangle spin and orbital angular momentum. The results from

these tests may help to improve understanding the fundamental nature of OAM vortex wave propagation.

6.2 Penetration and Reflection Tests

These experiments would test the ability of the phased-array OAM system to launch and receive penetrating radar waves, Figure 23. The OAM testbed as presently configured is bigger than most ground and wall penetrating radars. Nonetheless, the size is manageable for penetration and reflection tests, especially if the size is further reduced. Within the constraints of the present equipment, there are two primary methods of further reducing the size. One is to mount the antennas closer to one another and examine whether they are still able to produce a vortex. The other is to mix the signals up to higher frequencies, e.g. 2-3 GHz and use smaller antennas which would lead to a smaller array.

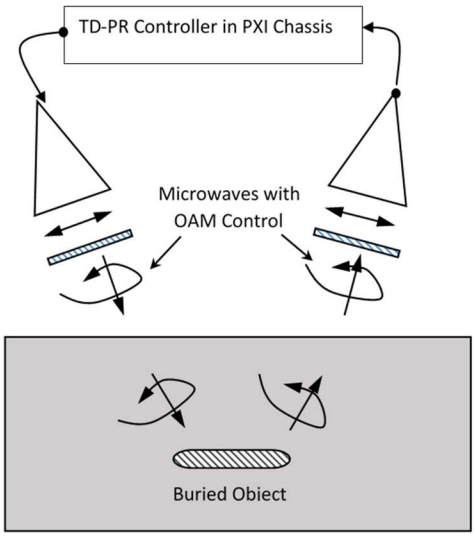

Figure 23. Bi-static OAM penetrating radar test configuration

Penetrating radars can make good use of antenna arrays to obtain more data faster, to reduce the need for antenna movements, multi-static reception and phased-array beam steering. Unwanted cross-coupling between antennas can degrade performance and limit test configurations. One method to achieve greater test flexibility with arrays is to use the orthogonality of different OAM modes to separate information flows. Processing the signals may require alternative methods, such as the concentric rings technique [Lin 2016].

6.3 OAM Interaction with Corners, Obstructions and Congested Subsurface Features

The results appearing in Figure 20 and Figure 22 indicate that vortex beams containing OAM may interact differently with obstructions than beams without OAM. If this result bears out, it may extend to similar geometric features, such as corners and around corners, and congested subsurface features. A set of relatively simple experiments complemented by numerical models would test this hypothesis.

6.4 Magnetron for OAM Generation

The magnetron is a mainstay of microwave signal generation that uses Helmholtz resonator excitation of cylindrical chambers by a swirling beam of electrons to create the microwave signal. The conventional magnetron uses only one of several resonating chambers to feed the microwave antenna. Due to the possibility of controlling the relative phase of the resonating chambers, it may be possible to use feed lines from the multiple chambers with controlled phase to generate the signals for an OAM source array, Figure 24.

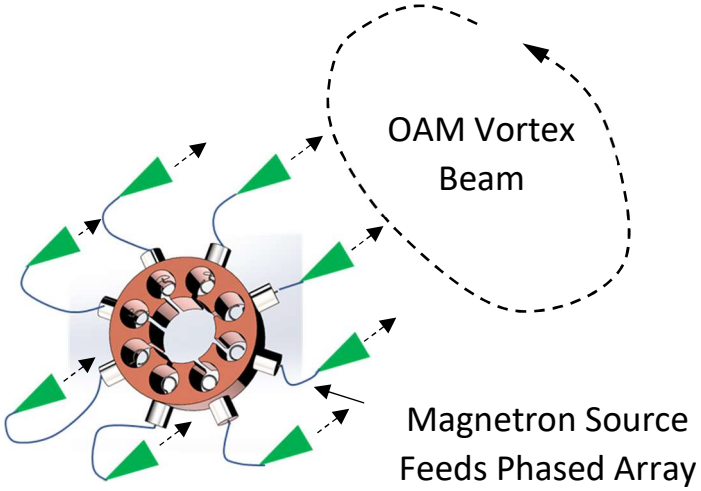

Figure 24 Magnetron with multiple chambers using relative phase to serve as a source for an OAM array.

6.5 Combined OAM Radar and Communications

OAM EM waves can serve dual roles – radar and communications. In some cases it may be possible to combine radar and communications signals from a single source. Combined radar and communications signals have been proven viable for conventional non-OAM waves. This research would explore extending the combination technique to OAM waves.

6.6 Possible Quantum Radars

Several techniques may be possible:

HOM Interferometer and Ghost Imaging

The Hong-Ou-Mandel (HOM) interferometer is a common test of entangled bosons that can be incorporated into sensors with relatively minimal complexity. One approach for radar is to first verify the performance of an entangling schemes with a conventional HOM interferometer. This would be followed by a system that combines OAM with a non-OAM wave as described in the optical regime by Ndagano [2019].

Hyperentangled OAM Sensing
The time-domain microwave and OAM control instruments may be of use in developing hyperentangled OAM sensing systems along the lines described by Smith III [2015]. These tests would require additional components to entangle the microwave photons. One possibility may be to insert nonlinear and/or elements into an auxiliary resonator ring chamber attached to the top of the phased array magnetron in Figure 24. Metamaterials have been shown to be a viable method of entangling photons at optical wavelengths [Stav 2018]

Testing and Development of Microwave Idlers and Optical to Microwave Converters.
A primary challenge is the control and sensing of microwave photons, which have considerably less energy and different material interactions than corresponding optical photons. A series of devices have been proposed and developed to control the quantum state of microwave photons. Many of which use optical to mechanical to microwave conversion at cryogenic temperatures, especially the time domain devices. Alternatives that may be more promising for practical radar applications include frequency domain devices, such as rings and nonlinear combs, which entangle larger numbers of photons via their wavelengths.

Compressive Sensing with Frequency-Domain Entangled Microwaves
If the frequency domain entanglement of microwaves can be realized then it may be possible to conduct frequency-domain compressive sensing experiments similar to the time-domain optical compressive sensing system developed by Howland [2014].

Quantum Doppler Sensing
Similarly, if the frequency domain entanglement of microwaves can be realized it should be possible to build and test quantum Doppler radars to verify the performance enhancements, i.e. and clutter rejection capability and low power operation suggested by [Lanzagorta 2016].

7. Additional Support with Projects of Interest to DOD

This research contract is for the purchase of equipment and accessories only. It does not contain funding for the conduct of experiments. Some of the above-described experiments using this equipment received support from other sources. A graduate research fellowship to University of Vermont Mechanical Engineering Ph.D. student Dan Orfeo from the Vermont Space Grant Consortium under NASA Cooperative Agreement NNX15AP86H helped with conducting the described experiments. Additionally, some of the components for the OAM testbed came from a U.S. Army SBIR Phase II award, entitled “Multi-static Ground Penetrating Radar for Buried Explosive Hazard Detection” with White River Technologies, Contract Number W909MY-17-C-0020.

8. Publications

Research using equipment acquired as part of this project has appeared in the following conference publications:

Orfeo D, Ezequelle W, Xia T, Huston DR. (2019) "Orbital Angular Momentum Assisted Ground Penetrating Radar" SPIE Defense + Commercial Sensing Symposium Detection and Sensing of Mines, Explosive Objects, and Obscured Targets XXIV, paper no. 11012-47, Baltimore, MD, DOI:10.1117/12.2520545

Orfeo D, Burns D, Xia T, Huston D. (2019) "Phased Array for Control of Orbital Angular Momentum in Microwave Systems" IEEE 2019 IEEE International Symposium on Phased Array Systems and Technology, Waltham, MA, USA

9. Summary and Conclusions

This project has been completed largely as proposed. Microwave test equipment capable of producing and measuring microwaves with potential OAM content has been acquired. The equipment works as expected. Experiments with the equipment indicate that it may be possible to produce microwave beams with OAM using phased-array techniques and that these beams may exhibit behaviors behind obstructions that differs from beams without OAM.

References

Allen EH, Karageorgis M, Riga JM (2008) "Sensor Systems and Methods using Entangled Quantum Particles" US Patent 7,767,976

Allen L, Beijersbergen MW, Spreeuw RJ, Woerdman JP. (1992) "Orbital Angular Momentum of Light and the Transformation of Laguerre-Gaussian Laser Modes" Phys. Rev. A 45, 8185

Andrews RW, Peterson RW, Purdy TP, Cicak K, Simmonds RW, Regal CA, Lehnert KW. (2014) "Bidirectional and Efficient Conversion between Microwave and Optical Light," Nature Phys. 10, 321, DOI: 10.1038/NPHYS2911

Barzanjeh S, Guha S, Weedbrook C, Vitali D, Shapiro JH, Pirandola S. (2015) "Microwave Quantum Illumination" Phys Rev Lett 114, 080503

Barzanjeh S, Abdi M, Milburn GJ, Tombesi P, Vitali D. (2012) "Reversible Optical-to-Microwave Quantum Interface" Phys. Rev. Lett. 109, 130503

Cheng GL, Chen AX, Zhong WX. (2012) "Entanglement of tripartite microwave radiation via quantum coherence in single molecular magnets" Journal of the Optical Society of America B Vol. 29, 6, 1376-1382, doi:10.1364/JOSAB.29.001376

Cheng L, Hong W, Hao ZC. (2014) "Generation of Electromagnetic Waves with Arbitrary Orbital Angular Momentum Modes" Scientific Reports 4, Article number: 4814, doi:10.1038/srep04814

Durnin J. (1987) "Exact Solutions for Nondiffracting Beams. I. The Scalar Theory" J Opt Soc Am, 4, 4, 651- 654

Howland GA. (2014) "Compressive Sensing for Quantum Imaging" PhD Dissertation, Department of Physics and Astronomy, University of Rochester, Rochester, NY, 2014

Jack B, Leach J, Romero J, Franke-Arnold S, Ritsch-Marte M, Barnett SM, Padgett MJ. (2009) "Holographic Ghost Imaging and the Violation of a Bell Inequality" Phys Rev Lett 103, 083602

Lanzagorta M. (2012) Quantum Radar, Morgan & Claypool Publishers

Lanzagorta M, Jitrik O, Uhlmann J, Venegas S. (2016) "Clutter Attenuation using the Doppler Effect in Standoff Electromagnetic Quantum Sensing" Proc. SPIE 9829, Radar Sensor Technology XX, 98291E, doi:10.1117/12.2223972

Lin M, Gao Y, Liu P, Liu J. (2016) "Improved OAM-Based Radar Targets Detection Using Uniform Concentric Circular Arrays" International Journal of Antennas and Propagation, Volume 2016, Article ID 1852659

Lloyd S. (2008) "Enhanced Sensitivity of Photodetection via Quantum Illumination," Science 321, 1463

Lopaeva ED, Ruo Berchera I, Degiovanni IP, Olivares S, Brida G, Genovese M. (2013) "Experimental Realization of Quantum Illumination" Phys. Rev. Lett. 110, 153603

Mazeas F, Traetta M, Bentivegna M, Kaiser F, Aktas D, et al. (2016) "High Quality Photonic Entanglement for Wavelength-Multiplexed Quantum Communication Based on a Silicon Chip" Optics Express, Optical Society of America, 2016, 24 (25), pp.28731-28738

Messiah A. (1965) Quantum Mechanics, Volume II, John Wiley & Sons, New York, 507-577

Ndagano B, Forbes A. (2019) "Entanglement Distillation by Hong-Ou-Mandel Interference with Orbital Angular Momentum States" APL Photonics 4, 016103

Pauli W. (1940) "The Connection Between Spin and Statistics" Phys Rev Vol 58, 716

Pu M, Li X, Ma X, Wang Y, Zhao Z, Wang C, Hu C, Gao P, Huang C, Ren H, Li X, Qin F, Yang J, Gu M, Hong M, Luo X. (2015) "Catenary Optics for Achromatic Generation of Perfect Optical Angular Momentum" Science Advances, 1, 9, e1500396, DOI: 10.1126/sciadv.1500396

Ren H, Li X, Zhang Q, Gu M. (2016) "On-Chip Noninterference Angular Momentum Multiplexing of Broadband Light" Science, 352, 6287, 805-809

Roslund J, Medeiros de Araújo R, Jiang S, Fabre C, Treps N. (2014) "Wavelength-Multiplexed Quantum Networks with Ultrafast Frequency Combs" Nature Photonics 8, 109–112, doi:10.1038/nphoton.2013.340

Saleh BE, Teich ME. (1991) Fundamental of Photonics, Wiley, New York, 45-51

Smith III JF. (2015) "Sensors based on quantum hyper-entanglement: efficiency and performance in the presence of other photon sources" Quantum Information and Computation XIII, E Donkor, AR Pirich, M Hayduk, Proc. of SPIE Vol. 9500, doi: 10.1117/12.2176245

Smith JF. (2017) "Using Hyperentanglement to Enhance Resolution, Signal-to-Noise Ratio, and Measurement Time" Optical Engineering 56(3), 031210, DOI: 10.1117/1.OE.56.3.031210

Smith III JF. (2009) "Quantum Entangled Radar Theory and a Correction Method for the Effects of the Atmosphere on Entanglement" Proc. SPIE 7342, Quantum Information and Computation VII, 73420A (April 27, 2009); doi:10.1117/12.819918

Stav T, Faerman A, Maguid E, Oren D, Kleiner V, Hasman E, Segev M. (2018) "Quantum Entanglement of the Spin and Orbital Angular Momentum of Photons using Metamaterials" Science, 361, 6407, 1101-1104.

Stellinga D, Pietrzyk ME, Glackin JM, Wang Y, Bansal AK, Turnbull GA, Dholakia KD, Samuel ID, Krauss TF. (2018) "An Organic Vortex Laser" ACS Nano, 12 (3), 2389–2394

Tan SH, Erkmen BI, Giovannetti V, Guha S, Lloyd S, Maccone L, Pirandola S, Shapiro JH. (2008) "Quantum Illumination with Gaussian States," Phys. Rev. Lett. 101, 253601

Xia K. (2015) "Deterministic Generation of Bright Multicolor Entanglement from Optomechanical Systems" arXiv:1507.07310v1

Yuan T, Wang H, Cheng Y, Qin Y. (2017) "Electromagnetic Vortex-Based Radar Imaging Using a Single Receiving Antenna: Theory and Experimental Results" Sensors 2017, 17(3), 630; doi:10.3390/s17030630

Wangsness RK. (1986) Electromagnetic Fields, 2nd ed., Wiley, New York, 359-361